JOURNAL OF GEOPHYSICAL RESEARCH, VOL. 104, NO. C8, PAGES 18,047–18,057, AUGUST 15, 1999

# Velocity and transport of the Labrador Current determined from altimetric, hydrographic, and wind data

Guoqi Han and C. L. Tang

Coastal Ocean Sciences, Fisheries and Oceans Canada, Bedford Institute of Oceanography, Dartmouth Nova Scotia, Canada

**Abstract.** Seasonal change of velocity and transport in the Labrador Current is studied using 3.5 years of TOPEX/Poseidon altimeter data, in conjunction with concurrent wind data and climatological density data. A method based on the linearized momentum equation is developed, in which vertically averaged velocities and volume transports normal to selected sections across the Labrador Sea are computed with the sea surface being the level of known motion measured by the altimeter. The three data sources have significantly different temporal and spatial scales, and thus a smoothing technique has been applied to ensure their consistency. Error analyses are performed to estimate the uncertainty in altimetric measurements and geophysical corrections and in density data. The seasonal range of the Labrador Current transport from the 300-m isobath seaward to the deepest ocean varies from 17 Sv at the Nain Section to 10 Sv at the Hamilton Section and 5 Sv at the northern Newfoundland Section, with a maximum in winter or fall and a minimum in spring. The barotropic effect associated with sea surface slope is most important over the shelf break and upper continental slope at the Nain and Hamilton Sections. At the northern Newfoundland Section the baroclinic effect associated with density gradients has a magnitude comparable with that of the barotropic effect. The largest baroclinic variability occurs offshore of the main density front over the lower continental slope of the Hamilton Section. The Ekman transport variability forced by local wind stress is negligible.

## 1. Introduction

The Labrador Sea is a region of the North Atlantic of increasing interest to oceanographers in recent years because of the important role it plays in water mass formation, thermohaline circulation, and possibly climate change. The circulation of and the main current in the Labrador Sea, the Labrador Current, have been studied by many investigators over the past 20 years. The residual circulation in the western Labrador Sea was studied by *LeBlond et al.* [1981] using moored measurements, satellite-tracked surface buoys, and geostrophic calculations. *Clarke* [1984], using density data, current observations, and various ad hoc assumptions, estimated that the westward transport into the Labrador Sea south of Cape Farewell was ~34 Sv (Sv $\equiv 10^6$ m$^3$ s$^{-1}$). *Thompson et al.* [1986], using the topographic Sverdrup relationship and climatological monthly-mean wind data, found that the Sverdrup transport in the Labrador Sea (mainly trapped in the lower continental slope) has a mean value of 37 Sv and an annual range of ~6 Sv, maximum in February and minimum in November. A wind-driven barotropic model of the North Atlantic by *Greatbatch and Goulding* [1989] indicated that the transport from the coast to the 3000-m isobath had the maximum in January and the minimum in July, with a difference of ~5 Sv. *Lazier and Wright* [1993], using long-term current meter measurements, conductivity-temperature-depth (CTD) data, and certain assumptions about the deep currents, estimated the mean summer transport shoreward of the 3000-m isobath at the Hamilton Bank at 11 Sv, with an annual range of 4 Sv. A diagnostic calculation by *Reynaud et al.* [1995] gave a basin-scale transport of the Labrador Sea of 49 Sv and a Labrador Current transport of 19 Sv in summer. *Tang et al.* [1996], using a diagnostic model and surface currents data derived from ice beacon, found a winter transport of 53 Sv in the Labrador Sea circulation.

The major uncertainty in transport estimates using hydrographic data is the specification of the level of no motion. Long-term current meter data help to reduce the uncertainty, but the number of current meter moorings in the Labrador Sea were too few to allow an accurate determination of the spatial variation of deep currents. Regional numerical models can produce both sea surface elevation and three-dimensional current fields, but the results are boundary-condition dependent, and the accuracy of transport estimates from models depends critically on the amount of current data available for model calibration. In this study, we develop a method based on data only to calculate currents and transports without using a priori assumptions such as the level of no motion. This is possible because sea surface slope, a missing component in the traditional methods of calculations, can now be calculated directly from satellite altimetry such as that from TOPEX/Poseidon.

Applications of satellite altimeter data, in general, fall into two categories: (1) temporal analysis of variability of the sea surface height and (2) absolute height determination referenced to an ocean geoid. Although both require accurate altimetric measurements, the former is independent of the geoid. The accuracy of altimetric sea surface height above a reference ocean geoid depends on altimeter measurements and their corrections, the reference ocean geoid model, and the satellite orbit measurements. While many of the corrections have been made on the basis of models, the largest errors

Published in 1999 by the American Geophysical Union.

Paper number 1999JC900145.

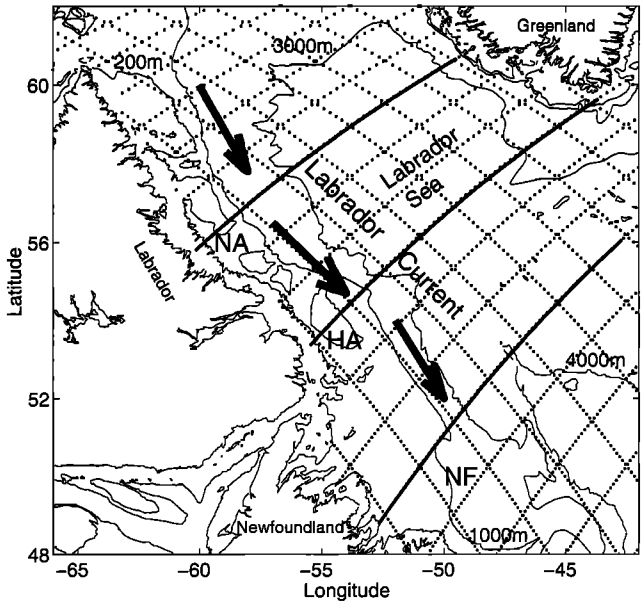


**Figure 1.** Map showing the study area. The dotted lines denote the ascending (up eastward) and descending (down eastward) TOPEX/Poseidon ground tracks. Three transects (thick lines) across the Labrador Sea are selected for analysis in this study: the Hamilton (HA), Nain (NA), and northern Newfoundland (NF) Sections. The 200-m, 1000-m, 3000-m, and 4000-m isobaths (thin lines) and the location of the Labrador Current (thick arrows) are also shown.

are associated with the geoid and ocean tides. For application of altimeter data in the Labrador Sea, *Han and Ikeda* [1996] studied annual variability of the sea surface topography using the TOPEX/Poseidon and Geosat altimeter data. Their results indicated predominance of the steric height effect over the wind-driven barotropic response in the altimetric height variability in the deep Labrador Sea.

In this study, we use the TOPEX/Poseidon altimeter data, coupled with density and wind data, to study the velocity and transport in the Labrador Sea circulation with a focus on the Labrador Current. Particular care is taken to match the temporal and spatial scales in these data. The combined use of sea surface elevation and density data allows a unique determination of the velocity and transport, in which the sea surface is the level of known motion derived geostrophically from the altimeter data. The scientific issues addressed in the paper include the seasonal variation of the transport and velocity of the Labrador Sea circulation, the individual contributions to the transport from surface slope, density gradients, and local winds, and the variation of the transport along the Labrador continental slope. To achieve these objectives, an ascending ground track of TOPEX/Poseidon from the Hamilton Bank to Cape Farewell (henceforth referred to as the Hamilton Section, Figure 1) was selected for detailed analysis since abundant hydrographic data along the track including observations from Ocean Weather Station Bravo (56.5°N, 51°W) were available. Analysis was also carried out for two other ascending tracks as shown in Figure 1, which were designated as the Nain Section and the northern Newfoundland Section. The advantage of the along-track analysis over a two-dimensional analysis [e.g., *Han and Ikeda*, 1996] is that no additional mapping errors are introduced. Furthermore, the selected ascending tracks are approximately perpendicular to the Labrador Current, so the along-track analysis is an appropriate choice.

This paper is divided into six sections. Section 2 briefly describes the preprocessing techniques of TOPEX/Poseidon altimeter, density, and wind data. Mathematical details for the computation of velocities, smoothing techniques, and error estimates are given in section 3. Section 4 examines the seasonal variability of velocity and transport of the Labrador Current. A comparison of our results with other work is discussed in section 5. Section 6 summarizes the findings of the study.

## 2. Data

### 2.1. TOPEX/Poseidon Altimeter Data

A subset of the TOPEX/Poseidon altimeter data of the merged geophysical data records (MGDR) produced by the Jet Propulsion Laboratory (JPL), from December 1992 to April 1996, is used in this work. The satellite repeats its ground tracks every 9.9156 days, thus giving ~120 cycles of data at each location under ideal conditions. However, the actual number of data points is smaller over the Labrador Shelf mainly because of ice coverage during winter.

Raw altimeter data with an along-track resolution of 5.9 km were edited using quality flags and parameter ranges recommended by JPL [*Benada*, 1993]. Corrections were made to account for various instrumental, atmospheric, and some oceanographic effects using the values provided in the MGDR. The atmospheric corrections include the ionospheric delay and the wet and dry tropospheric delays. The sea state bias, the inverse barometric response of the sea surface to the atmospheric pressure change, and the ocean, Earth, and pole tides were among the oceanographic corrections. The standard Goddard Space Flight Center precise orbit based on the joint gravity model-2 (JGM-2) were used.

Since the geoid is time-invariant, we separated time-varying height anomalies from mean heights. The mean surface heights were computed only at grid points where more than 40 cycles of the corrected sea surface height data were available, and the sea surface height anomalies were then calculated with the means removed. The data set for the altimetric height anomalies was divided into four seasons: winter (January, February, and March), spring (April, May, and June), summer (July, August, and September), and fall (October, November, and December). The altimetric seasonal height anomalies are independent of the geoid and the associated errors, and the errors in the oceanic tide correction are significantly reduced by the seasonal multiyear averaging (see section 3).

The altimetric sea surface height anomalies on the Hamilton Section are shown in Figure 2. The ascending-track data show horizontal gradient anomalies, upward in winter and fall and downward in spring and summer toward the Labrador coast. Relatively less data are available over the Labrador Shelf and upper slope in winter and spring, causing an increase of the standard errors. The standard errors are typically ~2 cm but increase to 6 cm over the shelf break and upper slope in winter, where the data were obtained mainly in early January before the water was covered by ice. Although the data shortage in the shelf region is severe for winter, the results presented in sections 4 and 5 are not gravely biased, since we are interested in the currents and transports offshore of the shelf break and the bulk of the transport of the Labrador Current is contributed by currents over the continental slope. Also presented in Figure 2 are sea surface height anomalies on the descending tracks

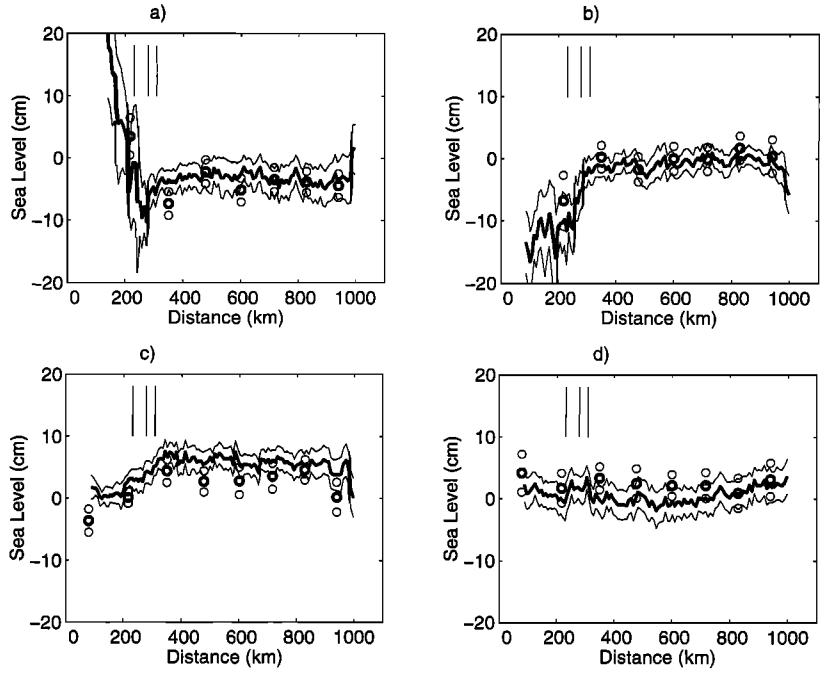


**Figure 2.** Seasonal sea surface height anomalies on the Hamilton Section in (a) winter, (b) spring, (c) summer, and (d) fall. The thick lines are the ascending-track data. The thick circles are the descending-track data at crossover locations (see Figure 1), with standard errors shown in thin circles. The thin lines indicate the standard errors of the seasonal-mean anomalies on the ascending track. The vertical lines indicate the locations of the 300-m (left), 1400-m (middle), and 2500-m (right) isobaths.

crossing the Hamilton Section. These crossover points provide a check on the quality of the altimetric height anomalies. Assuming that errors in the ascending-track data are independent of those in the descending-track data, we estimate a standard measurement error of ~2 cm, consistent with the value from the analysis of the ascending-track data. The random measurement and small-scale features in the altimetric data were removed by smoothing with a Cartwright filter (see section 3).

The mean sea surface elevation was calculated relative to the OSU91A geoid model in the MGDR. A Canadian geoid model GSD95 [*Veronneau*, 1995] was also used in order to examine the sensitivity of the mean transport to geoid models (see section 5).

### 2.2. Density Data

Density was computed from a seasonal data set of temperature and salinity for the northwest Atlantic of *Tang and Wang* [1996]. This data set was compiled using an iterative difference-correction procedure and a depth dependent domain of averaging. The data source is the Atlantic Fisheries Adjustment Program (AFAP) historical temperature and salinity database archived at the Bedford Institute of Oceanography. The database covers an area from northern Baffin Bay to Cape Hatteras and from the coast to 42°W and includes data from a variety of sources dating back to 1910. The data are divided into the same four seasons as the altimeter data are. Ideally, seasonal density data over the same three and a half years period as that for the altimeter data should be used, but the amount of hydrographic data is far from sufficient for such a calculation. Figure 3 shows the summer surface temperature and salinity. Note that the Hamilton Section has particularly dense data. For winter and fall the data are sparser but still adequate for this study. Bilinear interpolation was used to interpolate the density onto the selected transects. The density distribution on the Hamilton Section (Figure 4) clearly shows large horizontal density gradients over the shelf break and upper slope where the core of the traditional Labrador Current is located. Stratification of the upper water column is strongest in summer and weakest in winter.

### 2.3. Wind Data

Wind data from December 1992 to April 1996 were obtained from the National Centers for Environmental Prediction–National Center for Atmospheric Research (NCEP-NCAR) reanalysis project [*Kalnay et al.*, 1996], which produced 6-hourly 10-m wind velocity with a spatial resolution of 1.875° in longitude by 1.904° in latitude. The quadratic stress law of *Large and Pond* [1981] was used to compute wind stresses from the wind velocities. The computed wind stresses were averaged over the same period as the TOPEX/Poseidon data was to obtain the seasonal-mean values and interpolated bilinearly onto the selected sections.

## 3. Velocity and Transport Computation Method

In this section, we show how the altimetric data can be used in conjunction with the density and wind data to compute the depth-averaged normal velocity and transport from the momentum equation. With the nonlinear, local acceleration and horizontal friction terms neglected, the equation for velocity $v$, perpendicular to a vertical transect, reads

$$-fv = -\frac{1}{\rho_0}\frac{\partial p}{\partial l} + \frac{1}{\rho_0}\frac{\partial \tau}{\partial z} \tag{1}$$

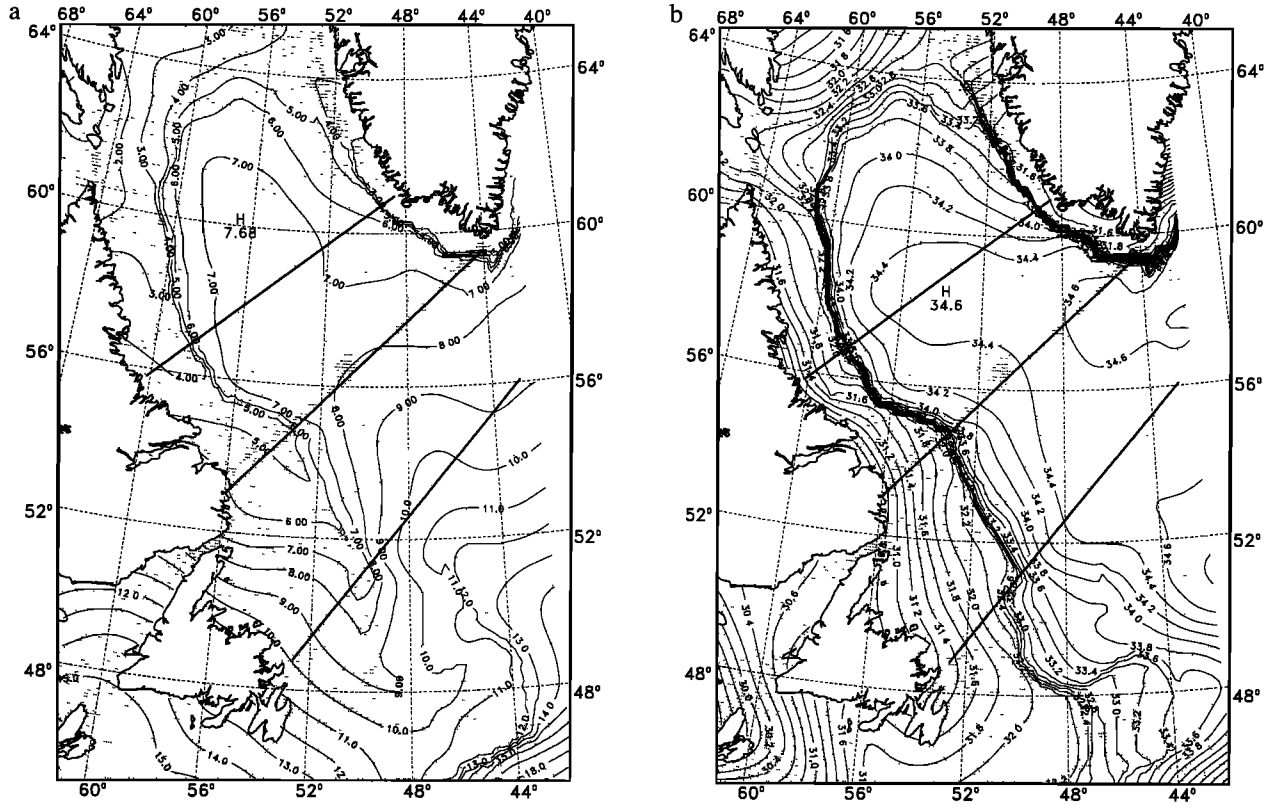


**Figure 3.** Summer conditions in the northwest Atlantic: (a) sea surface temperature (in °C) and (b) sea surface salinity. The dots indicate data points in a 5′ by 5′ grid. The Hamilton, Nain, and northern Newfoundland Sections are shown as solid lines.

$$p = g\rho_0\zeta + g\int_z^0 \rho\, dz \tag{2}$$

where $v$ is positive northward, $l$ is the horizontal coordinate along the section with $l = 0$ at the Labrador coast increasing offshore, $f$ is the Coriolis parameter, $p$ is the pressure, $z$ is the vertical coordinate positive upward with $z = 0$ at the still water level, $g$ is the gravity acceleration, $\rho$ is the density of water, $\rho_0$ is the reference density, $\tau$ is the along-transect component of the shear stress, and $\zeta$ is the sea surface height referenced to an ocean geoid, adjusted for the local atmospheric pressure.

Integrating (1) and (2) over the depth and neglecting the bottom stress term, we get the vertically averaged velocity:

$$V = \frac{g}{f}\frac{\partial\zeta}{\partial l} + \frac{g}{f}\frac{\partial\phi_1}{\partial l} + \frac{g}{fH}\frac{\partial\phi_2}{\partial l} - \frac{1}{\rho_0 fH}\tau_0 \tag{3}$$

$$\phi_1 = \frac{1}{g}\int_{-H}^0 b\, dz \qquad \phi_2 = \frac{1}{g}\int_{-H}^0 bz\, dz \tag{4}$$

$$b = (g/\rho_0)[\rho(l, z) - \bar{\rho}(z)] \tag{5}$$

where $V$ is the depth-averaged velocity normal to the transect, $b$ is the buoyancy parameter, $H$ is the local water depth, $\tau_0$ is the along-track component of surface wind stress, and $\bar{\rho}(z)$ is a reference density obtained by averaging $\rho$ at a given depth across the transect. We group the terms on the right-hand side of (3) into three components, $V_s$ (the first term), $V_t$ (the second and third terms), and $V_E$ (the fourth term), corresponding to the contributions from sea surface slope, density, and local wind stress, respectively.

By definition, the surface current (not including the Ekman current) is also given by $V_s$. An integration of $HV_t$ over the horizontal distance along the section is the contribution of the currents relative to the surface current to the total transport. Hereinafter, we refer to $V_s$ as the barotropic flow, $V_t$ as the baroclinic flow, and $V_E$ as the Ekman flow. We note that the designation of barotropic and baroclinic flows is a matter of definition. Some authors [e.g., *Mellor et al.*, 1982] define the current just above the bottom boundary layer as barotropic flow, which is called bottom current in this paper. The bottom current can be calculated from

$$v(-H) = \frac{g}{f}\frac{\partial\zeta}{\partial l} + \frac{1}{f}\int_{-H}^0 \frac{\partial b}{\partial l}\, dz \tag{6}$$

Equation (6) shows that a part of the density effect is reflected on the bottom current.

The advantage of the present definition of the barotropic and baroclinic flows is that the effects due to sea surface slope and density can be discussed in a more satisfactory way. $V_t$ involves only density and thus is mainly controlled by thermodynamic processes and advection. Sea surface slope at the boundaries of the Labrador Sea is set up by the large-scale circulation and wind field. As the water moves around the basin, the sea surface slope adjusts itself in such a way that all conservation laws are satisfied. Sea surface slope and thus $V_s$ are indirectly related to but not explicit functions of density.

The altimeter, density, wind, and bottom depth data have different spatial resolutions (see section 2). To ensure their consistency in the spatial scales, $\zeta$, $\phi_1$, $\phi_2$, and $H$ were

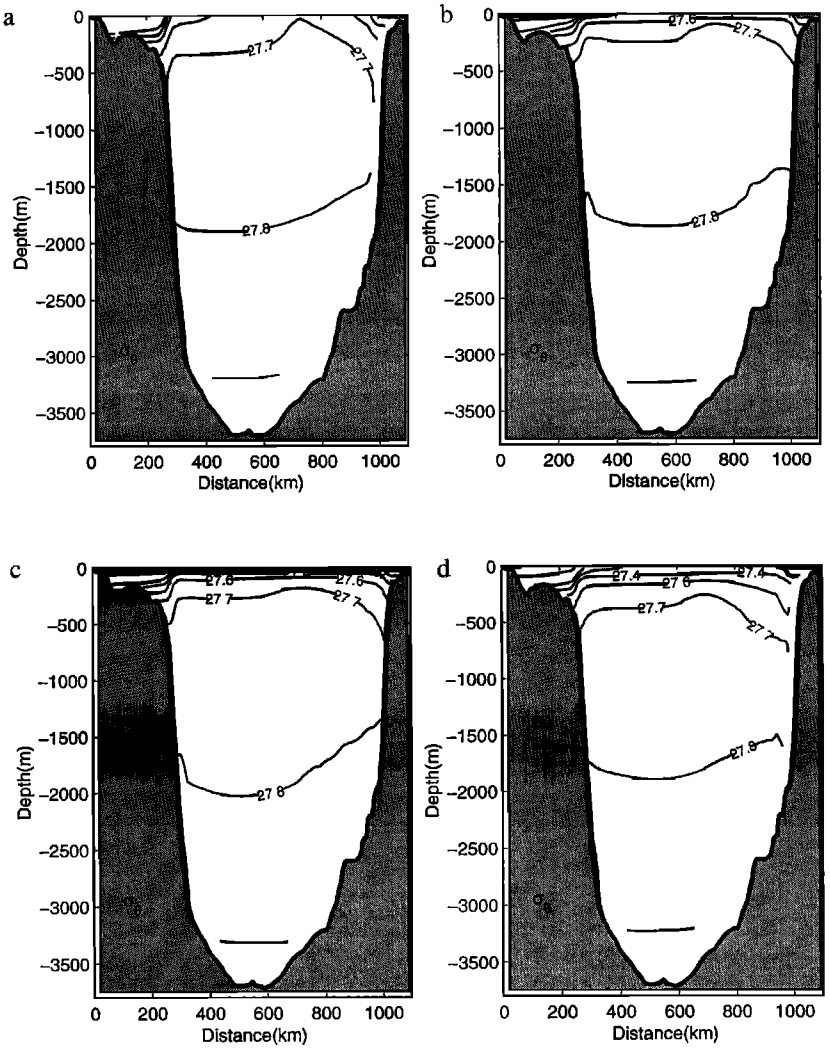


**Figure 4.** Potential density (in kg $m^{-3}$) distribution across the Hamilton Section for (a) winter, (b) spring, (c) summer, and (d) fall. The contour intervals are 0.5 kg $m^{-3}$ for density below 27.0 kg $m^{-3}$, 0.1 kg $m^{-3}$ for density above 27.6 kg $m^{-3}$, and 0.2 kg $m^{-3}$ otherwise.

smoothed by a Cartwright filter with a 200-km cutoff wavelength in the along-section direction. Filtering reduces high wave number random noises but, at the same time, decreases the horizontal resolution of the calculated currents. The baroclinic Labrador Current over the shelf break and upper slope has an instantaneous width of ~50 km [*Lazier and Wright*, 1993], but its seasonal-mean signature is expected to be wider because of the shifting of the axis of the current. With the half-cutoff wavelength of 100 km we expect that the baroclinic Labrador Current obtained from the filtered data would be much broader than its instantaneous width. The horizontally integrated transport, however, is less sensitive to the cutoff wavelength as long as the bounds for the calculation are sufficiently broad. A spectral analysis of the altimetric sea surface height indicates that the seasonal variability is dominant at wavelength 200 km or longer. Another aspect of filtering is that it shortens the data at the two ends of the section. As a consequence, there are no data at locations shoreward of the 300-m isobath after filtering with the cutoff wavelength of 200 km. Previous studies [e.g., *Lazier and Wright*, 1993] indicated that the core of the baroclinic Labrador Current was located at the 1000-m isobath and that the transport from the 400-m to 1200-m isobath accounted for 85% of the transport over the shelf and upper slope. Hence the shortening of data would not significantly affect the robustness of the results in this study.

The accuracy of the calculated currents depends on the accuracy of the sea surface slope. For seasonal anomalies, which are independent of the geoid, the error in sea surface slope was estimated using an ad hoc method in analogy to the linear regression theory. We assumed that the errors as shown in Figure 2 at each location in the seasonal altimetric height anomalies were uncorrelated, and we calculated the standard errors of slope over a data segment. Since we are only interested in features of length scales greater than 100 km (the half-cutoff wavelength), we used data segments of 100 km in the error estimates. The calculated standard errors represent the maximum errors, which vary with location and season. The largest errors are found at the shelf break and upper slope in winter, around 6 cm/100 km, which is equivalent to a standard error in the geostrophic surface current of 5 cm $s^{-1}$ at 55°N. The errors in velocity in summer and fall and in the central Labrador Sea are smaller, typically 1–2 cm $s^{-1}$.

The above error values are probably underestimates for the barotropic current error since there are spatially correlated

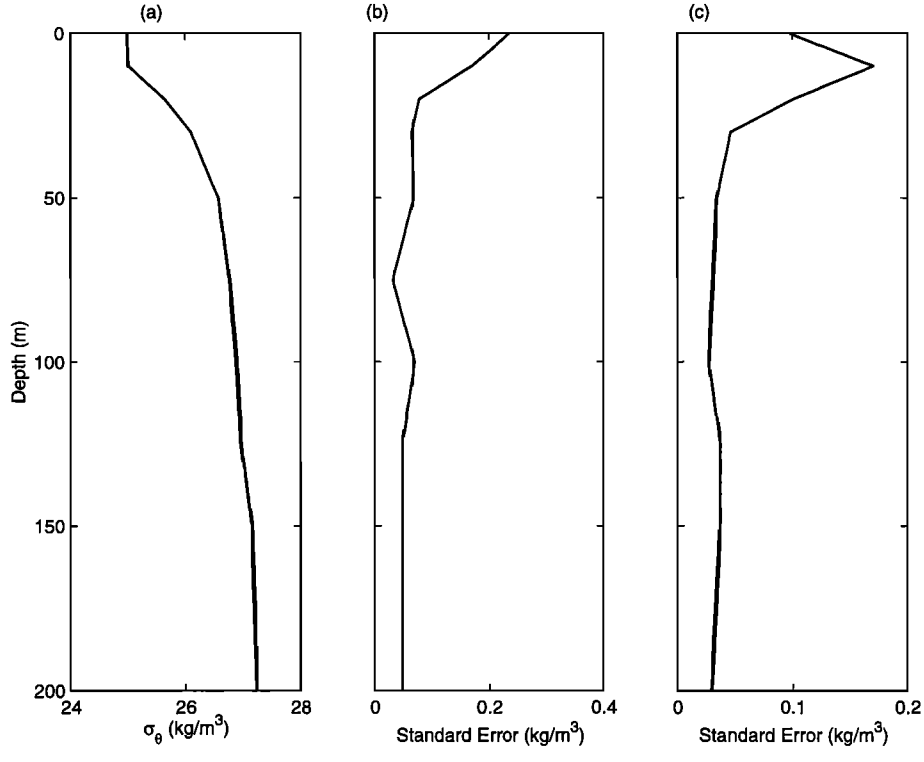


**Figure 5.** Vertical profiles showing (a) the climatological seasonal-mean density structure averaged over a small shelf area centered at 55°W and 54°N in summer, (b) the standard error measuring the uncertainty of density introduced from the interannual variability in the climatological data, and (c) the standard error measuring the uncertainty from the interannual variability in the 1993–1996 data.

errors associated with the atmospheric and oceanographic corrections to altimeter height measurements. These errors occur primarily at scales of ~1000 km. *Fu et al.* [1994] and *Tsaoussi and Koblinsky* [1994] discussed in detail errors in the altimeter measurements, the atmospheric and oceanographic corrections, and the orbit determination. Here we present an error estimate of the sea surface slope due to these correlated errors, based mainly on the values from the two studies. According to Fu et al., the error induced by the skewness of the ocean surface is estimated to be 1.2 cm, and that due to the electromagnetic bias is estimated to be 2.0 cm. The accuracies of the ionospheric, dry tropospheric, and wet tropospheric corrections are 0.5, 0.7, and 1.1 cm, respectively. The inverse barometric effect is estimated to be 2.8 cm [*Tsaoussi and Koblinsky*, 1994]. The error in the *Cartwright and Ray* [1990] ocean tide model has a global value of ~5 cm and is significantly reduced by the 3-month multiyear seasonal averaging since major semidiurnal and diurnal tidal constituents have aliasing periods less than 3 months. An exception is for the $K_1$ tide, which has an aliasing period of 173 days and a global error of 2.0 cm. The present seasonal averaging can reduce the $K_1$ error to less than 1.0 cm. The systematic component of the orbit error which is correlated geographically and which cannot be reduced by time averaging is estimated to be less than 2 cm. In consideration of its primary spatial scale of ~10,000 km, the orbit error is negligible in the present error estimation. The root-sum-square value of the above contributing error estimates gives a total error of 4.0 cm ($(1.2^2 + 2.0^2 + 0.5^2 + 0.7^2 + 1.1^2 + 2.8^2 + 1.0^2)^{0.5} = 4.0$ cm). With the dominant half wavelength of ~500 km the error in the sea surface slope is calculated to be 0.8 cm/100 km, equivalent to a current error of 0.7 cm s$^{-1}$. The total error associated with altimeter data may be given in terms of root-sum-square of the uncorrelated error estimated in the preceding paragraph and the correlated error. As we can see, the former dominates in the total error over the shelf break and upper continental slope in winter, while the latter may be a considerable part of the total error in summer and fall and in the central Labrador Sea.

The density data [*Tang and Wang*, 1996] were obtained from a nonlinear procedure based on the methods of *Levitus* [1982] and *Reynaud et al.* [1995], and hence a quantitative estimation of the velocity error associated with the density data is difficult. Here we make an order of magnitude estimation using raw data archived at the Bedford Institute. We have chosen a shelf location near the Hamilton Section (a 20 km by 20 km square centered at 55°W and 54°N) where there are sufficient data in summer for the error estimation. We first considered the uncertainty resulted from nonconcurrent density data. The period from 1925 to 1996 was divided into 18 4-year subperiods. The last subperiod is approximately coincident with the duration of the TOPEX/Poseidon and the NCEP-NCAR wind data used in this study. The 4-year means (not shown) and the climatological (entire period) mean (Figure 5a) were computed using available density data in this square area. Standard errors of density (Figure 5b) were estimated from deviations of the 4-year mean about the climatological mean. The standard error calculated in this way is due to interannual variability and an approximate measure of the error introduced by the use of climatological data. By using these standard errors of density we estimated standard errors in $\phi_1$ and $\phi_2$ from (4) and associated current errors over the 100-km segment. Their root-sum-square is the estimated current error due to the use of the

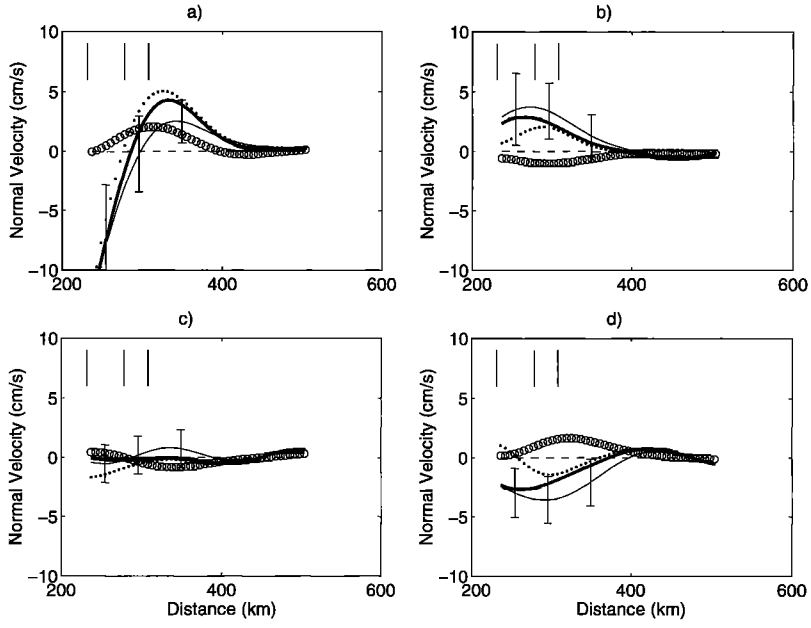


**Figure 6.** Normal velocity anomalies (in cm $s^{-1}$) on the Hamilton Section in (a) winter, (b) spring, (c) summer, and (d) fall. The total velocity anomalies (thick lines) are the sum of the barotropic flow $V_s$ (thin lines), depth-averaged baroclinic flow $V_t$ (open circles) relative to the surface current, and depth-averaged flow due to local winds (dashed lines). The bottom currents are shown as dotted lines. The standard errors (vertical bars) associated with the altimetric sea surface slope are also displayed. Note that the standard error of the baroclinic flow is 0.8 cm $s^{-1}$. The vertical lines indicate the locations of the 300-m (left), 1400-m (middle), and 2500-m (right) isobaths.

climatology. We then calculated a standard error of density due to interannual variability for the 1993–1996 period concurrent with the T/P and NCEP-NCAR data (Figure 5c), from which a current error is also estimated. Finally, the root-sum-square of the two error components gives a total error of ~0.8 cm $s^{-1}$ over the 100-km segment.

## 4. Seasonal Variation in the Labrador Current

### 4.1. Hamilton Section

Figure 6 shows the seasonal anomalies of the depth-averaged velocity on the Hamilton Section. The velocity anomalies were calculated relative to the mean velocities computed using the spring, summer, and fall velocities. The winter data were excluded from the calculation of mean velocities to avoid contamination of the results by large errors associated with the winter data. Since only relative velocities are considered here, the choice of the reference season(s) is not important. For instance, we could use summer as the reference season. The computed anomalies would then be all relative to summer.

The areas of large current anomalies are limited to within 400 km from the coast. Seasonal variability in the deep central Labrador Sea is small, consistent with *Han and Ikeda*'s [1996] finding. Compared to the contributions from sea surface slope and density gradient, the local wind stresses have very small effects on the seasonal variability, a result also found in numerical models [e.g., *Reynaud et al.*, 1995; *Tang et al.*, 1996]. The southward anomaly of the Labrador Current shoreward of the 1400-m isobath is largest in winter (note the large standard error, 5 cm $s^{-1}$) and fall and smallest in spring. Since the Labrador Current is a southward flowing current (negative velocity), a negative anomaly indicates enhancement and a positive anomaly indicates reduction of the current.

The barotropic flow exhibits a strong seasonal variation over the shelf break and upper continental slope (300–1400 m). The winter and fall anomalies have large negative values, indicating a strong surface current in these seasons. In contrast, the baroclinic flows have maximum magnitudes over the lower slope (1400–2500 m) and are negative in spring and summer (enhancement) and positive in winter and fall (reduction). The largest baroclinic variability over the lower slope offshore of the main density front (though the mean baroclinic current is largest across the density front [*Lazier and Wright*, 1993]) is interesting. On one hand, the main density front over the upper slope does not have a strong seasonal variation in the horizontal gradient (Figure 4). On the other hand, in the upper ocean just offshore the main density front the horizontal gradient is much larger in fall and winter than it is in spring and summer. In the lower water column the isopycnals in the opposite direction are steeper in spring and summer than they are in fall and winter. The net effect is much larger horizontal gradients in fall and winter than in spring and summer over the lower continental slope.

The transport anomalies over the shelf break and upper continental slope have a seasonal range of 5 Sv (Figure 7a). Note that a negative anomaly indicates an enhancement of the southward Labrador Current transport and that a positive anomaly indicates a reduction. Hence the result shows a larger transport in winter and fall and a smaller transport in spring. Because of the large barotropic error (3.7 Sv), we are less certain about the winter transport than we are about the transports in the other seasons. The contribution from the barotropic flow is much greater than that from the baroclinic flow. Over the lower continental slope, the transport has a smaller seasonal range, 3 Sv (Figure 7b). The baroclinic effect increases the transport in spring and summer and decreases the

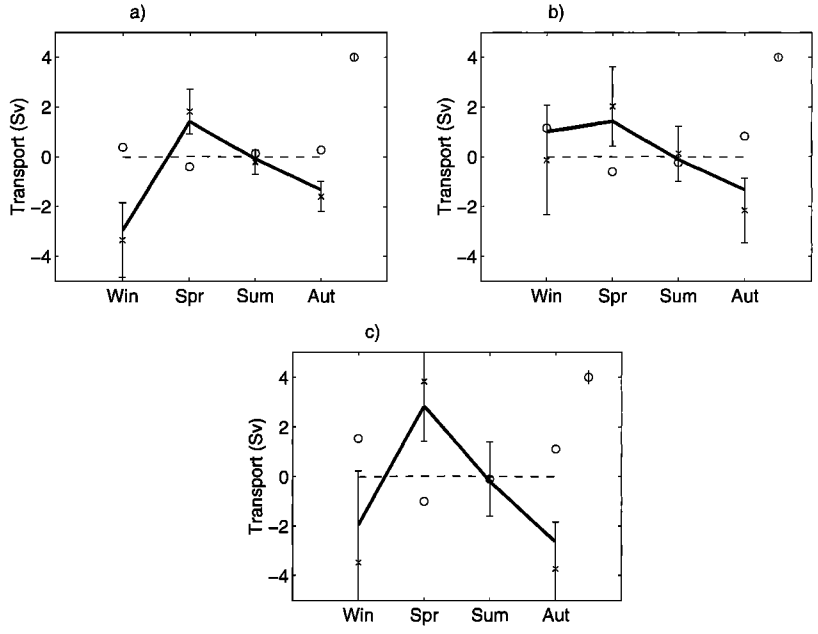


**Figure 7.** Volume transport anomalies for the Hamilton Section over (a) the upper slope from 300 to 1400 m, (b) the lower slope from 1400 to 2500 m, and (c) the upper and lower slopes from 300 to 2500 m. The total transport (thick lines) is the sum of the barotropic (crosses), baroclinic (open circles), and wind-driven (dashed lines) components. The standard errors associated with the altimetric sea surface height anomaly (vertical bars) and with the density (vertical lines in the upper right corner) are also shown.

transport in fall. The total transport on the Hamilton Section from the 300- to 2500-m isobath has a seasonal range of 6.5 Sv (Figure 7c). A similar calculation indicates that the seasonal range from the 300-m isobath to the deepest sea is 10 Sv (not shown). Overall, the barotropic contribution from sea surface slope dominates the seasonal transport variability. The baroclinic effect is more important over the lower slope than it is over the upper slope.

### 4.2. Nain and Northern Newfoundland Sections

The calculations for the Hamilton Section were repeated for the Nain and northern Newfoundland Sections (see Figure 1). The results for the horizontally integrated transports are shown in Figures 8 and 9. Comparing the results of the three sections, we find that the seasonal variations of the total transport are similar, largest in winter and fall and smallest in spring.

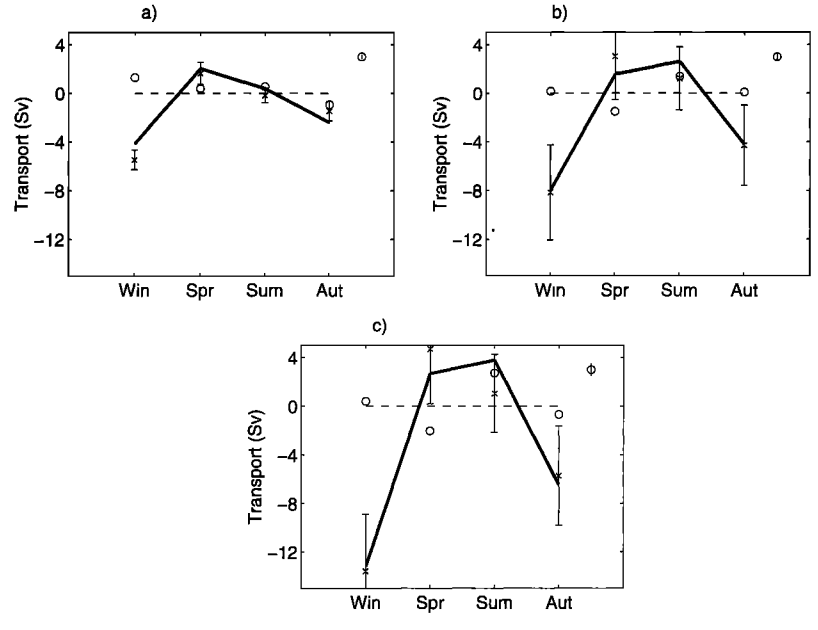


**Figure 8.** Same as Figure 6 but for the Nain Section.

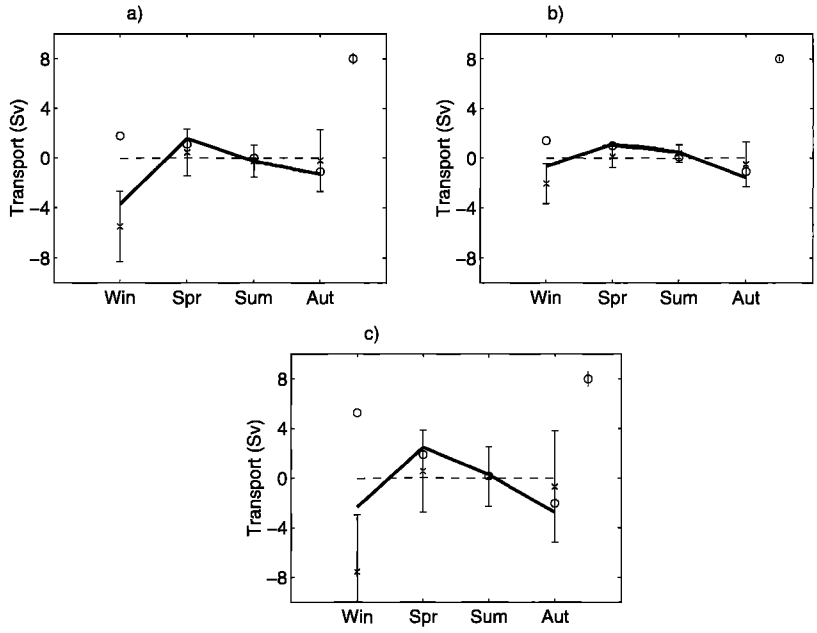


**Figure 9.** Same as Figure 6 but for the northern Newfoundland Section.

The most prominent difference among the three sections is the significant reduction in the seasonal range from 17 Sv at the Nain Section to 6.5 Sv at the Hamilton Section (300- to 2500-m isobath). Considering that the transport variability may not be limited to the 2500-m isobath, we extended the integration of transport seaward to the deepest ocean and found that the transports at the Nain and northern Newfoundland Sections (5 Sv) changed little but that the transport at the Hamilton Section was increased from 6.5 to 10 Sv. The decreasing transport from north to south can be related to the circulation pattern in the southwestern Labrador Sea. Observations and numerical models [*Lazier*, 1994; *Tang et al.*, 1996] indicate that the Labrador Current branches off the continental slope north of the Hamilton Section (56°N, 52°W) and recirculates in the northwestern Labrador Sea and that a northward countercurrent originating from the North Atlantic Current exists off the Newfoundland slope (52°N, 46°W). These currents act to reduce the longshore transport of the seasonal-mean gyre circulation and the associated seasonal transport variation.

Comparing the barotropic and baroclinic effects, we find that the barotropic effect is dominant at the two northern sections from 300 to 1400 m, suggesting that this effect weakens seaward and southward. The baroclinic effect enhances the southward flow at Nain in spring, at Hamilton in spring and summer, and at northern Newfoundland Section in fall, indicating a southward propagation of the density effect (Figures 7b, 8b, and 9b). The propagation speed (estimated to be ~10 cm $s^{-1}$) has an order of magnitude comparable to the mean current speed from moored measurements of *Lazier and Wright* [1993].

The largest negative anomalies in the barotropic transport occur in winter for all three sections, which are associated with the large upward sea surface slope onshore. The increased sea surface slope in winter is also obtained from numerical models of the Labrador Sea [*Tang et al.*, 1996]. The barotropic contribution to the transport variability as reflected in sea surface slope is not only determined by large-scale meteorological forcing but is also influenced by density gradient. This influence is due to an inherent relation between the sea surface elevation and the density gradient, though not apparent in the linear equation used in the present transport calculation. At the northern Newfoundland Section the magnitude of the total transport anomaly in winter is much smaller than that of either the barotropic or baroclinic transport anomaly, suggesting that the large negative anomaly in the barotropic flow is mainly contributed by the local density gradient. At the Hamilton and Nain Sections the magnitude of the total transport anomaly in winter is very close to that of the barotropic anomaly, indicating that the contribution of the local density gradient to the barotropic transport anomaly is minor.

## 5. Discussion

From the diagnostic calculations presented in section 4 we have found that the seasonal variation of the transport across the Hamilton Section (Figure 7) has a range of 5 Sv to the 1400-m isobath and 6.5 Sv to the 2500-m isobath, that the maximum transport occurs in winter and fall, and that the minimum transport occurs in spring. Both the magnitude and phase of the seasonal variation are compatible with observations over both the upper and lower continental slopes of the Hamilton Section [*Lazier and Wright*, 1993]. Their current measurements show maximum currents in fall and winter and minimum currents in early spring and a transport range of 4 Sv from the coast to the 1400-m isobath.

The seasonal variation of the transport has been studied with models by several investigators. *Thompson et al.* [1986], using the topographic Sverdrup relationship and a climatological monthly wind field, found an annual range of ~6 Sv in the Sverdrup transport of the Labrador Sea (mainly trapped in the lower continental slope), maximum in February and minimum in November. *Greatbatch and Goulding* [1989] from a linear barotropic model driven by the Hellerman and Rosenstein climatological monthly wind stresses obtained a transport difference of ~5 Sv (from the coast to the 3000-m isobath), maximum in January and minimum in July. The differences

between the model results and this investigation can be caused by a variety of factors in model forcing: low spatial resolution of the wind field, lack of density variation in the model, and use of climatological wind fields.

We and other authors [*Reynaud et al.*, 1995] have shown that local winds play an insignificant role in the basin-scale transport of the Labrador Sea. The controlling factor of the seasonal transport variation is most likely the boundary inflow south of Greenland where the Eastern Greenland Current and Irminger Current in the upper and middle water column and the Denmark Strait overflow at the bottom flow westward to feed the Labrador Sea.

While the results presented in this study demonstrate the feasibility of the combined use of altimeter, hydrographic, and wind data to determine the currents and transports in the Labrador Sea, the exercise also reveals some limitations associated with data quality, availability, and processing procedure. Insufficient altimetric data over the Labrador Shelf and the upper continental slope in winter due to ice coverage limits the accuracy of seasonal transport calculations in winter. Given the substantial interannual variability of this region [e.g., *Deser and Blackmon*, 1993], the limited duration (~3.5 years) of altimetric observations could introduce considerable uncertainty in the calculated seasonal barotropic currents (reflected in their standard errors in Figure 2 and Figures 6–9). Furthermore, the use of climatological density data, instead of data concurrent with the T/P data period, introduces additional errors to the computed seasonal-mean density and therefore to the baroclinic flow component (section 3).

The method presented in this paper can also be used to compute the absolute seasonal-mean velocity and transport from altimetric, density, and wind data. A preliminary analysis in this study has indicated that the geoid error is a major factor of uncertainty in the determination of the absolute sea surface slope and surface currents at the scales of interest.

## 6. Conclusions

We have developed a method to compute currents and transports using altimeter data, density data, and wind data. The method allows a unique determination of the velocities and transports, for which the sea surface is the level of known motion measured by the altimeter. We have used the method to examine the Labrador Current and the Labrador Sea circulation, from TOPEX/Poseidon altimeter data, NCEP-NCAR wind data, and climatological AFAP density data. Special care has been taken to match the scales of the three data sources in a realistic way, and error analyses are performed to estimate the uncertainty associated with the TOPEX/Poseidon and density data. While the present study confirms many known features of the Labrador Current and the Labrador Sea circulation, it also reveals new features of interest.

The seasonal change of the depth-averaged current mainly occurs over the continental slope. The current variability in the deep central Labrador Sea is very weak. The results clearly indicate an enhancement of the Labrador Current in fall and a reduction in spring. For the Hamilton Section the barotropic flow has a strong seasonal cycle over the shelf break and upper continental slope, while the baroclinic variability is largest offshore of the main density front over the lower continental slope.

The ranges of the seasonal transport of the Labrador Sea gyre are 17, 10, and 5 Sv at the Nain Section, the Hamilton Bank Section, and the northern Newfoundland Section, respectively. The decreasing variability from north to south is attributed to the influence of the circulation pattern in the southwestern Labrador Sea in which an eastward current off the slope of the Hamilton Bank and a northward countercurrent off the slope of the northeast Newfoundland Shelf carry the water away from the Labrador Current. The Labrador Current transport from the 300- to 1400-m isobaths at the Hamilton Section has a seasonal range of 5 Sv, consistent with moored measurements. The southward transports in the Labrador Current and the basin-scale circulation are largest in winter and fall and smallest in spring, in agreement with available direct current observations and model results.

Variability of the transport is dominated by the barotropic (associated with sea surface slope) effect on the northern sections. For the northern Newfoundland Section the baroclinic (associated with density gradient) effect and barotropic effect have comparable magnitudes. The transport variability in the surface Ekman layer induced by local wind stress is insignificant compared with the barotropic and baroclinic components.

**Acknowledgments.** This work was supported by the Canadian Panel for Energy Research and Development. We are indebted to Brian Petrie and Tom Yao for reading an early version of the manuscript and giving helpful comments. Brendan DeTracey and C. K. Wang assisted in the analysis of hydrographic and wind data. Roland Schweitzer of NOAA Climate Diagnostics Center provided the wind data. We thank JGR reviewers for their helpful comments and suggestions. The TOPEX/Poseidon data were obtained from the NASA PODAAC at JPL, California Institute of Technology.

## References

Benada, R., Merged GDR (TOPEX/POSEIDON) users handbook, *JPL D-11007*, Jet Propul. Lab., Pasadena, Calif., 1993.

Cartwright, D. E., and R. D. Ray, Oceanic tides from Geosat altimetry, *J. Geophys. Res.*, *95*, 3069–3090, 1990.

Clarke, R. A., Transport through the Cape Farewell-Flemish Cap section, *Rapp. P. V. Reun. Cons. Int. Explor. Mer*, *185*, 120–130, 1984.

Deser, C., and M. L. Blackmon, Surface climate variations over the North Atlantic Ocean during winter: 1900–1989, *J. Phys. Oceanogr.*, *23*, 1743–1753, 1993.

Fu, L.-L., E. J. Christensen, C. A. Yamarone Jr., M. LeFebvre, Y. Menard, M. Dorrer, and P. Escudier, TOPEX/Poseidon mission overview, *J. Geophys. Res.*, *99*, 24,369–24,381, 1994.

Greatbatch, R. J., and A. Goulding, Seasonal variations in a linear barotropic model of the North Atlantic driven by the Hellerman and Rosenstein wind stress field, *J. Phys. Oceanogr.*, *19*, 572–595, 1989.

Han, G., and M. Ikeda, Basin-scale variability in the Labrador Sea from TOPEX/Poseidon and Geosat altimeter data, *J. Geophys. Res.*, *101*, 28,325–28,334, 1996.

Kalnay, E., et al., The NCEP/NCAR 40-year reanalysis project, *Bull. Am. Meteorol. Soc.*, *77*(3), 437–471, 1996.

Large, W. F., and S. Pond, Open ocean momentum flux measurements in moderate to strong winds, *J. Phys. Oceanogr.*, *11*, 324–336, 1981.

Lazier, J. R. N., Observations in the northwest corner of the North Atlantic Current, *J. Phys. Oceanogr.*, *24*, 1449–1463, 1994.

Lazier, J. R. N., and D. G. Wright, Annual velocity variations in the Labrador Current, *J. Phys. Oceanogr.*, *23*, 659–678, 1993.

LeBlond, P. H., T. R. Osborn, D. O. Hodgins, R. Goodman, and M. Metge, Surface circulation in the western Labrador Sea, *Deep Sea Res. Part A*, *28*, 683–693, 1981.

Levitus, S., Climatological atlas of the world ocean, *NOAA Prof. Pap. 13*, Natl. Oceanic and Atmos. Admin., Washington, D. C., 1982.

Mellor, G. L., C. R. Mechoso, and E. Keto, A diagnostic calculation of the general circulation of the Atlantic ocean, *Deep Sea Res. Part A*, *29*, 1171–1192, 1982.

Reynaud, T. H., A. J. Weaver, and R. J. Greatbatch, Summer mean circulation of the northwestern Atlantic Ocean, *J. Geophys. Res.*, *100*, 779–816, 1995.

Tang, C. L., and C. K. Wang, A gridded data set of temperature and

salinity for the northwest Atlantic Ocean, *Can. Data Rep. Hydrogr. Ocean Sci. 148*, iv + 45 pp., Fish. and Oceans Can., Ottawa, Canada, 1996.

Tang, C. L., Q. Gui, and I. K. Peterson, Modeling the mean circulation of the Labrador Sea and the adjacent shelves, *J. Phys. Oceanogr.*, *26*, 1989–2010, 1996.

Thompson, K. R., J. R. N. Lazier, and B. Taylor, Wind-forced changes in Labrador Current transport, *J. Geophys. Res.*, *91*, 14,261–14,268, 1986.

Tsaoussi, L. S., and C. J. Koblinsky, An error covariance model for sea surface topography and velocity derived from TOPEX/Poseidon altimetry, *J. Geophys. Res.*, *99*, 24,669–24,683, 1994.

Veronneau, M., The GSD95 geoid model for Canada, internal report, Geod. Surv. Div., Dep. of Nat. Resour., Ottawa, Canada, 1995.

G. Han and C. L. Tang, Coastal Ocean Sciences, Fisheries and Oceans Canada, Bedford Institute of Oceanography, Dartmouth, Nova Scotia, Canada B2Y 4A2. (ghan@emerald.bio.dfo.ca)

(Received January 22, 1998; revised April 20, 1999; accepted April 28, 1999.)